MAGNETOHYDRODYNAMICS Vol. 53 (2017), No. 4, pp. 653–665

ELECTROMAGNETIC INTERACTION BETWEEN A PERMANENT MAGNET AND LAMINAR FLOW OF A MOVING SPHERE IN A CONDUCTING LIQUID

Z. Lyu[1], *T. Boeck*[1], *C. Karcher*[1], *A. Thess*[2]

[1] *Institute of Thermodynamics and Fluid Mechanics, Technische Universität Ilmenau, P.O. Box 100565, D-98684 Ilmenau, Germany*

[2] *Institute of Engineering Thermodynamics, German Aerospace Center (DLR), Pfaffenwaldring 38-40, 70569 Stuttgart, Germany*

e-Mail: Ze.Lyu@tu-ilmenau.de

Lorentz force velocimetry (LFV) is a non-contact electromagnetic flow measurement technique for electrically conducting liquids. It is based on measuring the flow-induced force acting on an externally arranged permanent magnet. Motivated by extending LFV to liquid metal two-phase flow measurement, in a previous test we considered the free rising of non-conductive bubbles/particles in a thin tube of liquid metal (GaInSn) initially at rest. We observed that the Lorentz force signals strongly depend on the size of the bubble/particle and on the position where it is released. Moreover, the force signals cannot be reproduced in detail, which necessitates a statistical analysis. This is caused by chaotic trajectories due to the rising velocities of about ∼200 mm/s. Therefore, in this paper, we use an improved setup for controlled particle motions in liquid metal. In this experiment, the particle is attached to a straight fishing line, which suppresses any lateral motion, and is pulled by a linear driver at a controllable velocity (0–200 mm/s). For comparison, we solve the induction problem numerically using Oseen's analytical solution of the flow around a translating sphere that is valid for small but finite Reynolds numbers. This simplification is made since the precise hydrodynamic flow is difficult to measure or to compute. The aim of the present work is to check if our simple numerical model can provide Lorentz forces comparable to the experiments. Although Oseen's solution becomes inaccurate near the sphere for finite Reynolds numbers, it provides a fore-aft asymmetry of the flow and is globally well-behaved. It provides an upper limit to the measurement results. We recover the peak-delay of the Lorentz force signals as well.

Introduction. Two-phase flows in an electrically conducting liquid occur in a number of metallurgical processes. For example, in continuous casting of steel, argon bubbles are injected in order to prevent clogging of the submerged entry nozzle and to mix the melt in the mold. Hence, liquid metal two-phase flows are not only of fundamental interest but also of practical importance. Among the various methods to measure them [1], one promising candidate is Lorentz force velocimetry (LFV) [2, 3]. LFV is based on the electromagnetic induction when a static localized magnetic field is applied to a conducting liquid. The current density $\mathbf{j}$ is induced according to Ohm's law for moving conductors, i.e.

$$\mathbf{j} = \sigma(\mathbf{E} + \mathbf{u} \times \mathbf{B}), \tag{1}$$

where σ is the electrical conductivity of the liquid, $\mathbf{E}$ is the electric field, and $\mathbf{u}$ is the liquid velocity, respectively. In general, the magnetic field $\mathbf{B}$ is the sum of the applied magnetic field $\mathbf{B_0}$ and the secondary magnetic field $\mathbf{b}$. However, in our experiment, we have $\mathbf{B} \approx \mathbf{B_0}$ because of a very low magnetic Reynolds number (Rm$\sim 10^{-4}$). The induction problem can then be analyzed in the quasi-static limit [4], i.e. the back-reaction of the flow on the magnetic field is negligible. Therefore, the Lorentz force density can be defined by the simplified expression

$$\mathbf{f}_\mathrm{L} = \mathbf{j} \times \mathbf{B_0}. \tag{2}$$

In LFV, we measure the counter-force to this flow-braking Lorentz force, which acts on the permanent magnet. When a small permanent magnet is used, the measured force can be used to evaluate the local velocity in the vicinity of the magnet. Earlier work has demonstrated the capability of LFV to detect a particle rising in liquid metal at rest [5]. We observed that the Lorentz force strongly depends on the size of the bubble/particle. However, the free rising velocity and the particle trajectory cannot be controlled, which is problematic for the analysis of Lorentz force signals. Therefore, in this paper, we present the results obtained in an improved setup with controllable particle motions in liquid metal, by which we evaluate the reproducibility of the Lorentz force signals. Additionally, the results of a simple numerical model are compared with the experiments.

This paper is organized as follows: in Section 1 the experimental setup is explained. In Section 2 we present our numerical model. In Section 3 we present the experimental and numerical results and discuss them. The concluding remarks are given in Section 4.

1. Experimental setup. As shown in Fig. 1, the experimental setup consists of a plastic vessel ($60\times60\times400\,\mathrm{mm}^3$) filled with liquid metal GaInSn. The spherical particle made of plastic (6 mm diameter) is electrically non-conducting and fixed on the fishing line, which is pulled through the top and bottom holes of the vessel and moves in a 10-mm-distance in parallel to the left side wall. The velocity of the sphere is controlled by an additional linear driver, which provides speeds in the range of 0 to 200 mm/s. The effect of the moving fishing line is neglected because of its small size (0.1 mm in diameter). Our LFV consists of a $12\times12\times12\,\mathrm{mm}^3$ permanent magnet, which is installed at 10-mm-distance on the side of the liquid. Its magnetic flux density is measured by a Gauss meter and is shown in Fig. 2. The Interference-Optical-Force-Sensor (IOFS) [6] measures the x-component of the Lorentz forces induced by the displacement flow of liquid around the particle.

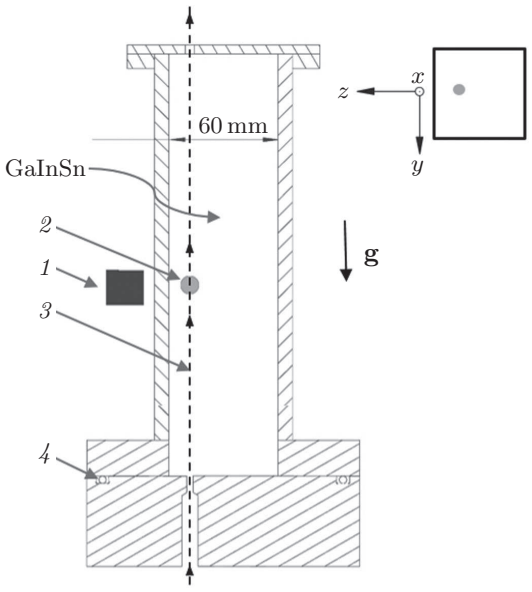

Fig. 1. Schematic of the experimental setup: *1* – LFV; *2* – spherical particle; *3* – fishing line; *4* – o-ring (top-view at the upper-right corner).

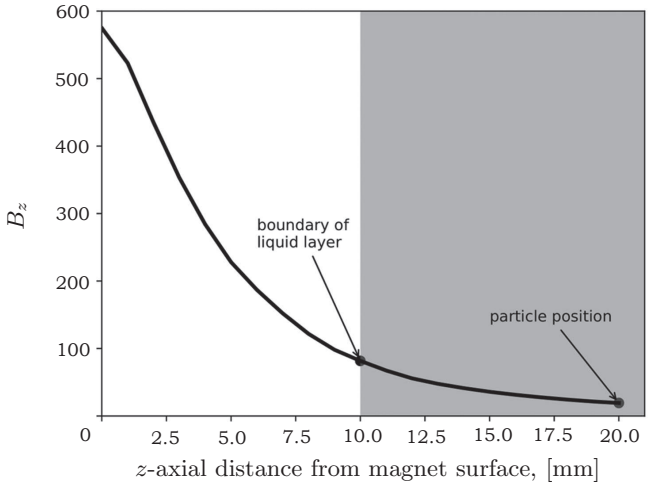

Fig. 2. The magnetic flux density B_z measured by the Gauss meter (at the particle position $B_z = 19.31$ mT.

The results of the particle velocity $u_0 = 10$ mm/s with a travelling distance of 283 mm are shown in this paper. Therefore, the particle Reynolds number Re_d can be estimated as follows

$$\mathrm{Re}_d = \frac{u_0 d\rho}{\mu} = 162.3, \tag{3}$$

where $d = 6$ mm is the diameter of the particle, $\rho = 6.492\,\mathrm{g/cm^3}$ is the density of GaInSn, and $\mu = 0.0024$ Pa·s is the dynamic viscosity of GaInSn, respectively. As expected, the magnetic Reynolds number Rm is small

$$\mathrm{Rm} = \mu_0 \sigma u_0 d = 2.6 \times 10^{-4}, \tag{4}$$

where μ_0 is the vacuum magnetic permeability, $\sigma = 3.46 \times 10^6\,\mathrm{S/m}$ is the conductivity of GaInSn at 20^oC, respectively. It suggests that the secondary magnetic field can be neglected in the numerical simulation due to $\mathrm{Rm} \ll 1$. For the Hartmann number Ha we obtain

$$\mathrm{Ha} = B_0 d \sqrt{\frac{\sigma}{\mu}} = 4.4, \tag{5}$$

where $B_0 = 19.31$ mT is the magnetic flux density at the center of the sphere (see also Fig. 2). This value demonstrates that in the present experiment the Lorentz force is comparable to viscous friction. Finally, to describe the ratio of the Lorentz forces to the inertial forces, we have the interaction parameter (Stuart number)

$$\mathrm{N} = \frac{\sigma B_0^2 d}{\rho u_0} = 0.12, \tag{6}$$

which is small in our experiments. We use the so-called "kinematic approach" [7] for our numerical simulation, although Ha is not small and may modify the flow near the boundaries. Here the velocity is prescribed by an analytical solution for the flow around a moving sphere.

2. Numerical model. The geometry of the numerical model is shown in Fig. 3, which is equivalent to the experiment. Here the domain of the liquid is a $60 \times 60 \times 400\,\mathrm{mm^3}$ rectangular cuboid. At 10-mm-distance on the side of it stays

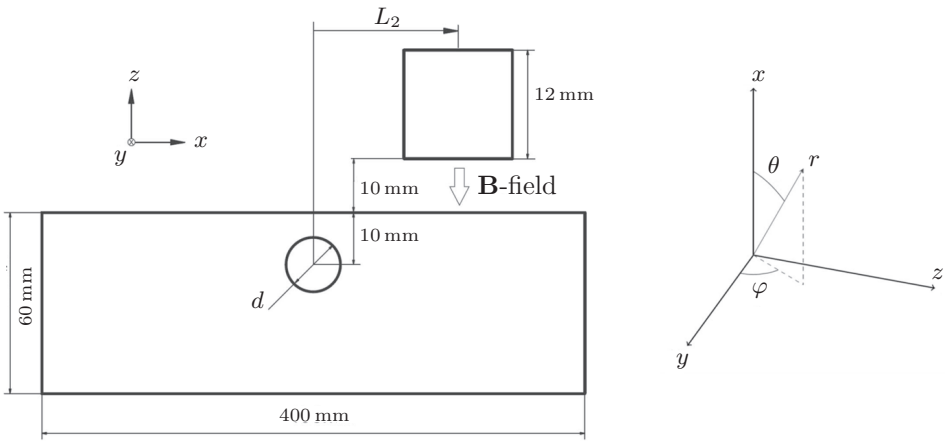

Fig. 3. Schematic of the geometry in simulation (view on the (x, z)-plane).

a cubic permanent magnet of 12 mm side-length. Inside the cuboid, there is a rigid sphere of $d = 6$ mm, which locates at 10-mm-distance to the liquid boundary. The x-axial distance between the magnet and the sphere in the simulation is $L_2 \in [-90, 90]$ mm.

We want to compute the electromagnetic induction of a pre-defined velocity field and a localized magnetic field. Thus, the governing equations read

$$\nabla^2 \Phi = \nabla \cdot (\mathbf{u} \times \mathbf{B_0}), \tag{7}$$

$$\mathbf{j} = \sigma[-\nabla \Phi + (\mathbf{u} \times \mathbf{B_0})], \tag{8}$$

$$\mathbf{f}_\mathrm{L} = \mathbf{j} \times \mathbf{B_0}, \tag{9}$$

where $\mathbf{u} = (u_x, u_y, u_z)$ is the velocity field in the reference system, and Φ is the electrical potential. The imposed magnetic field of the permanent magnet is calculated from the analytical solution presented by Furlani [8], which is determined by the integration of

$$\mathbf{B_0}(x, y, z) = \frac{\mu_0 M_\mathrm{s}}{4\pi} \sum_{k=1}^{2} (-1)^k \int_{y_1}^{y_2} \int_{x_1}^{x_2} \frac{(x-x')\mathbf{x} + (y-y')\mathbf{y} + (z-z_k)\mathbf{z}}{[(x-x')^2 + (y-y')^2 + (z-z_k)^2]^{3/2}} \mathrm{d}x' \mathrm{d}y'. \tag{10}$$

In Eq. (10), M_s is the surface magnetization of the magnet, (x_1, x_2), (y_1, y_2), (z_1, z_2) are the coordinates of the magnet's corners, $\mathbf{x}$, $\mathbf{y}$, $\mathbf{z}$ are the unit vector in the x-, y-, z-directions, respectively. To describe the velocity field using the analytical solutions, a spherical coordinate system is introduced and fixed in the center of the sphere (see Fig. 3):

$$x = r\cos\theta, \quad y = r\sin\theta\cos\phi, \quad z = r\sin\theta\sin\phi. \tag{11}$$

We use the analytical solutions of the flow generated by a sphere moving in the negative x-direction, which was originally found by Oseen [9, 10]. Usually it is represented as a Stokes stream function. The radial and angular components of velocity are

$$\begin{aligned} u_r &= -u_0 \frac{3ra^2 \exp\left\{\frac{r\mathrm{Re}}{2a}(\cos\theta - 1)\right\}\left(\frac{r\mathrm{Re}}{a}(1+\cos\theta)+2\right) - 2a^3\left(3\frac{r}{a}+\mathrm{Re}\cos\theta\right)}{4r^3\mathrm{Re}}, \\ u_\theta &= u_0 \frac{\sin\theta\left(3ar^2\exp\left\{\frac{r\mathrm{Re}}{2a}(\cos\theta-1)\right\}+a^3\right)}{4r^3}, \\ u_\phi &= 0, \end{aligned} \tag{12}$$

where r is the radial coordinate, $a = d/2$ is the sphere radius, and Re is one half of the particle Reynolds number Re_d, respectively. Then we implement Eq. (12) into our geometry as

$$\begin{aligned} u_x &= u_r\cos\theta - u_\theta\sin\theta, \\ u_y &= u_r\sin\theta\cos\phi + u_\theta\cos\theta\cos\phi, \\ u_z &= u_r\sin\theta\sin\phi + u_\theta\cos\theta\sin\phi. \end{aligned} \tag{13}$$

Finally, we may solve Eqs. (7)–(9) by implementing Eqs. (10)–(13), respectively, and obtain the reaction force $\mathbf{F}'_{\mathrm{L}}$ on the permanent magnet as

$$\mathbf{F}'_{\mathrm{L}} = -\int_V \mathbf{f}_{\mathrm{L}}\mathrm{d}V. \tag{14}$$

The simulations in this paper were done by the commercial code COMSOL Multiphysics. The finite Element Method (FEM) is used to determine the forces acting in the fluid. The solution domain is a rectangular cuboid with a sphere cut out. For this model, we use the hybrid tetrahedral mesh. In the computational domain, the elements are uniformly distributed over the x-axis. Smaller elements are applied in the region, where the gradient of the velocity field is large. The influence of discretization was examined by using meshes with different numbers of elements. The mesh used in subsequent computations in Section 3 is shown in Fig. 4. The effect of mesh quality on the Lorentz forces is checked and illustrated

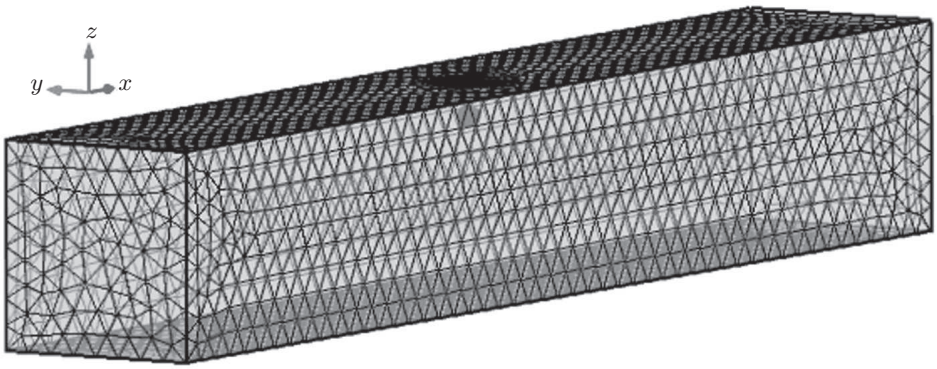

Fig. 4. Mesh used in simulations with 6.8×10^4 elements.

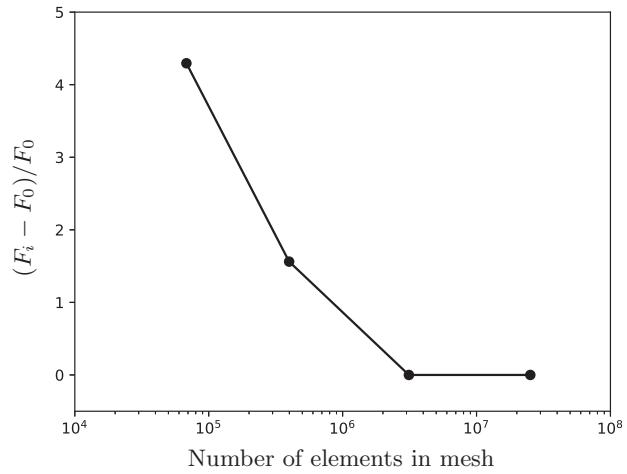

Fig. 5. Mesh study with $\mathrm{Re} = 0.01$, $u_0 = 10\,\mathrm{mm/s}$, at $L_2 = 0\,\mathrm{mm}$.

in Fig. 5, by which we show the deviation of the force amplitude of $(F_i - F_0)/F_0$, where F_0 is the is the x-component (axial) Lorentz force ($L_2 = 0$, $u_0 = 10\,\mathrm{mm/s}$, $\mathrm{Re} = 0.01$) in the case of maximum number of mesh elements. The influence of mesh quality on Lorentz forces is below 10^{-3}.

3. Results and discussion. The LFV measurement results of ten repeated cases of particle motion are shown in Fig. 6. With the particle velocity $u_0 = 10\,\mathrm{mm/s}$ and the particle travelling distance 283 mm, the actual travelling time of the particle is 28.3 s, during which we observed the "double peaks" of the Lorentz forces. In between these two peaks, the trough occurs at about 14.15 s, when the magnet is right at the $L_2 = 0\,\mathrm{mm}$ (zero position). Additionally, the first peaks are $2.3 - 3\,\mu\mathrm{N}$ and occur shortly before the $L_2 = 0\,\mathrm{mm}$ position, whereas the second peaks are $4 - 4.8\,\mu\mathrm{N}$ and are after the zero position. In such cases, we observed the good reproducibility of the force signals, which can hardly been seen in

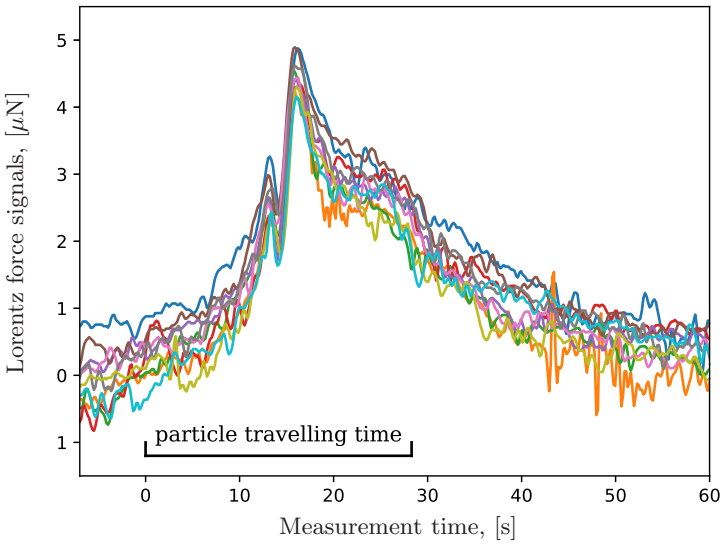

Fig. 6. Mesh study with $\mathrm{Re} = 0.01$, $u_0 = 10\,\mathrm{mm/s}$, at $L_2 = 0\,\mathrm{mm}$.

the previous study [5]. This is because the Reynolds number now (∼160) is much lower than that in the previous study (∼4000), and the wake behind the sphere is still a "Stable Vortex Region". According to Taneda [11], the vortex-ring in the wake of a sphere starts to oscillate at about $\mathrm{Re} = 200$. After 28.3 s the particle stops its motion, but there are still Lorentz force signals lasting about 20 s due to the remaining liquid motions in the vessel.

As for the numerical simulation, the analytical solutions of the flow around a translating sphere (Eqs. (12), (13)) were implemented. We set $u_0 = 10\,\mathrm{mm/s}$ and investigated the velocity profile depending on the Reynolds number. Although the Reynolds number should be depending on u_0, one may still be able to check the influence of the Reynolds number on the asymmetry of the flow by assuming a constant velocity and an adjustable viscosity. The velocity fields on the (x, z)-plane with $\mathrm{Re} = 0.1$, 1, 2, 5 are shown in Fig. 7, respectively. We observe that the velocity field around the sphere becomes more asymmetric as the Reynolds number increases. However, when $\mathrm{Re} > 1$, the velocity fields of the Oseen solution are significantly suppressed in the near-sphere region and becomes unphysical. Therefore, in the following results we are only interested in the cases of $\mathrm{Re} \leq 1$. It should be noted that Oseen's solution is derived for an unbounded flow around the sphere. In the present case, the velocity is non-zero on the walls, since the

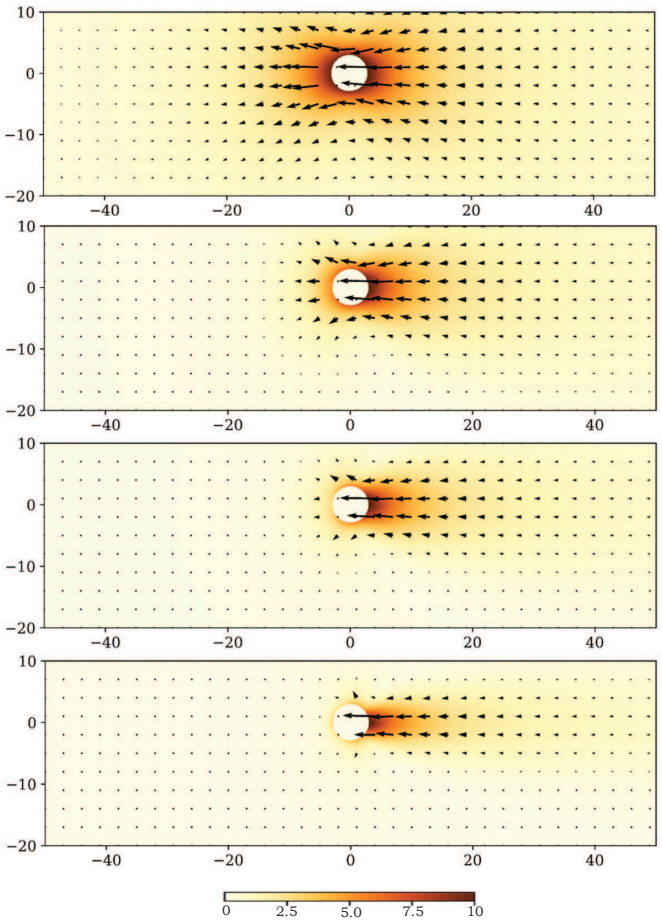

Fig. 7. The velocity field on the (x, z) plane ($u_0 = 10\,\mathrm{mm/s}$, contour of $\sqrt{u_x^2 + u_z^2}$ [m/s], from top to bottom $\mathrm{Re} = 0.1$, 1, 2, 5, respectively).

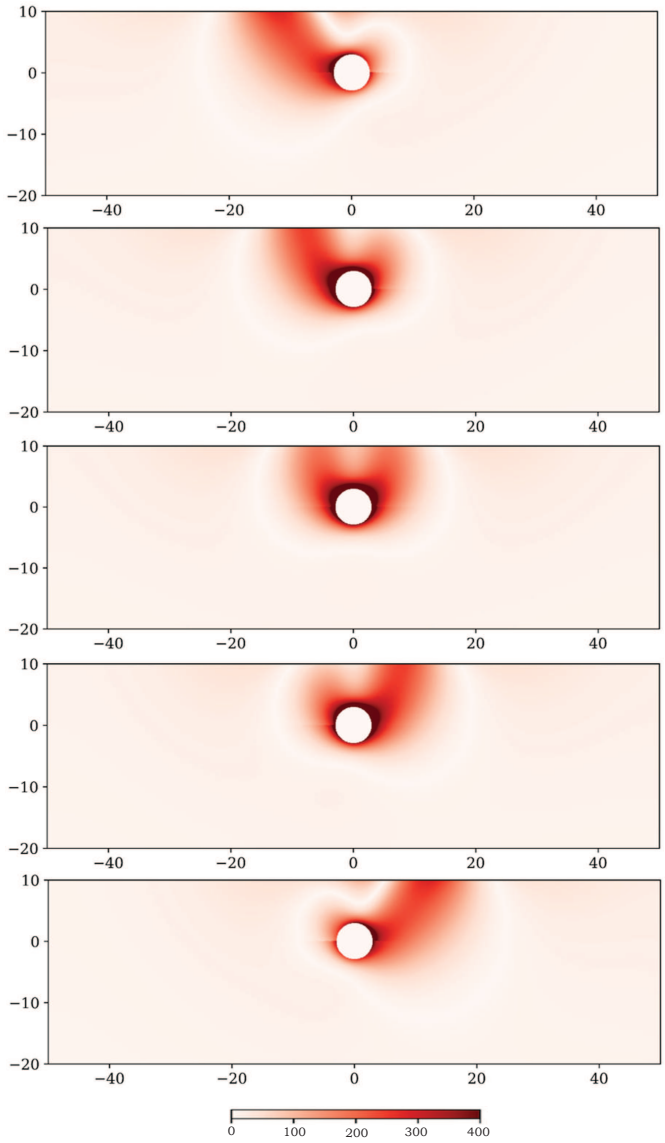

Fig. 8. Eddy current density distributions on the (x, z) plane ($\mathrm{Re} = 0.01$, contour of $\sqrt{j_x^2 + j_y^2 + j_z^2}$ [A/m^2], from top to bottom $L_2 = -10, -4, 0, 4, 10$ mm, respectively).

distance to the wall is not very large. We do not expect the analytical flow to correspond closely to the actual flows in the experiment. Nevertheless, it may be presumed that the relatively slowly decaying viscous velocity distributions provide an indication of the maximal force signals.

To reproduce the measurement cases, in the simulation model we set the permanent magnet to different locations (L_2) and observed the development of the eddy current density distributions and the Lorentz force density distributions, which are shown on the (x, z) symmetry plane ($x \in [-50, 50]$ mm, $z \in [-20, 10]$ mm) in Figs. 8–11, respectively. The eddy current density distributions of $\mathrm{Re} = 0.01$ are shown in Fig. 8 for $L_2 = -10, -4, 0, 4, 10$ mm, respectively. They show that the eddy currents are mainly induced in the near-magnet region and in the near-particle region, because the velocity and $\mathbf{B}_0$ are more significant there.

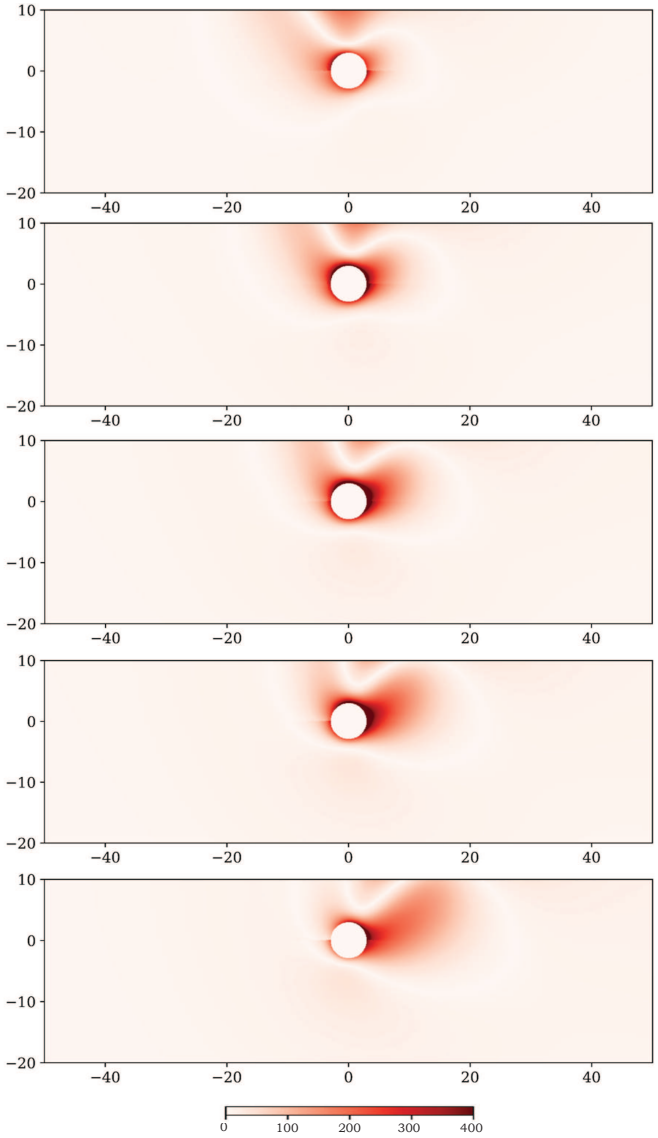

Fig. 9. Eddy current density distributions on the (x, z) plane ($\mathrm{Re} = 1$, contour of $\sqrt{j_x^2 + j_y^2 + j_z^2}$ [A/m^2], from top to bottom $L_2 = -10$, -4, 0, 4, 10 mm, respectively).

The distributions for L_2 and $-L_2$ are symmetrical about the "zero" position, because both the velocity and $\mathbf{B}_0$ are symmetric in this way. However, we observe the asymmetry of the eddy current density distributions in Fig. 9 for identical parameters except for $\mathrm{Re} = 1$. A more significant induction of the eddy current occurs downstream the "zero" position instead of that at the "zero" position. This is obviously caused by the asymmetric velocity field at $\mathrm{Re} = 1$. The Lorentz force density distributions of $\mathrm{Re} = 0.01$ are shown in Fig. 10, which similarly illustrates the symmetric distributions. Additionally, we observe more contribution of the Lorentz force density to the total force in the near-magnet region than that in the case of eddy current density distribution because of the large gradient of $\mathbf{B}_0$ in the z-direction. In Fig. 11 we see the Lorentz force density distribution for $\mathrm{Re} = 1$, which becomes asymmetric with respect to the "zero" position as well.

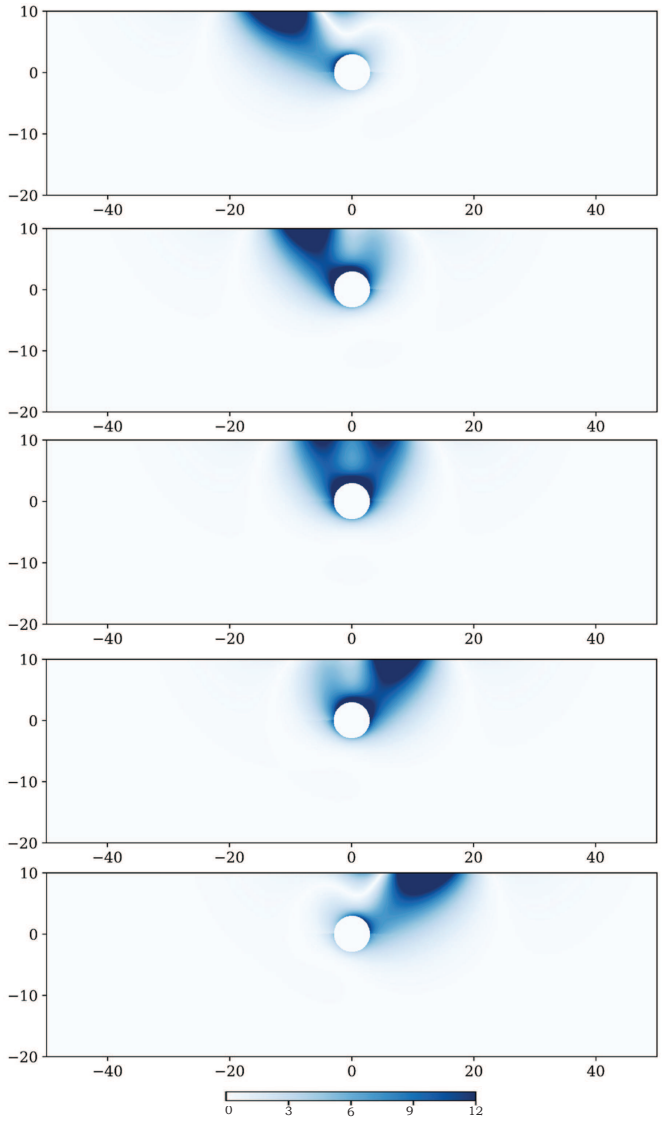

Fig. 10. Lorentz force density distributions on the (x, z) plane (Re = 0.01,, contour of $\sqrt{f_x^2 + j_y^2 + f_z^2}$ [N/m^3], from top to bottom $L_2 = -10$, –4, 0, 4, 10 mm, respectively).

From the simulation we obtained total Lorentz forces which depend on the axial distance L_2 between the magnet and the sphere. In order to compare the experimental and numerical results, the time t in the measurement was transformed to the distance L' by

$$L' = u_0(t - t_0), \tag{15}$$

where $t_0 = 14.15$ s is the middle time point of particle travelling in Fig. 6. Thus, the simulation and the experiment have the same "zero" position coordinate and can be compared in Fig. 12. The simulation showed that the Lorentz force peaks decreased as the Reynolds number increased. Additionally, we observed the trend of asymmetry depending on the Reynolds number. The higher the Reynolds number, the further the Lorentz force peak-position is to the "zero" position. It should be stressed that the results are physical only at low Reynolds number cases (Re ≤ 1).

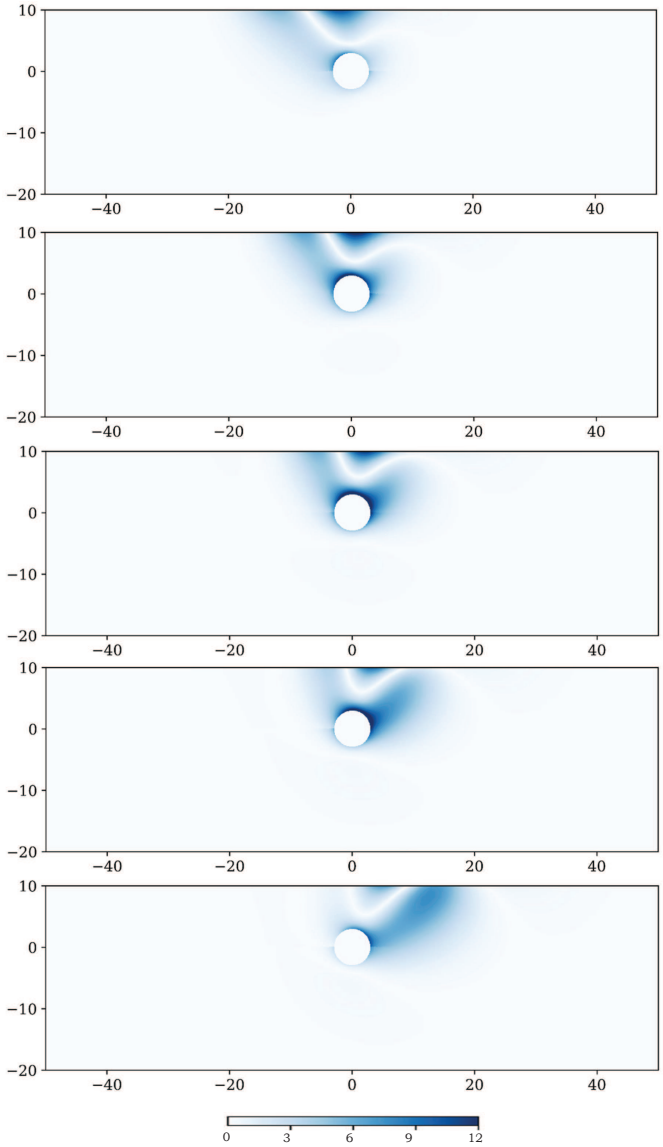

Fig. 11. Lorentz force density distributions on the (x, z) plane (Re = 1, contour of $\sqrt{f_x^2 + j_y^2 + f_z^2}$ [N/m^3], from top to bottom $L_2 = -10$, -4, 0, 4, 10 mm, respectively).

One measurement case (Re∼160) in Fig. 6 is shown in Fig. 12 as well. Unfortunately, the Reynolds number in the measurement is beyond the capability of our velocity solution, and thus we cannot do a one-to-one comparison. However, the measurement and the simulations together form a reasonable trend. Our model can provide the upper-limit of the Lorentz force for the experiment.

We extract the peak-position from the simulations and plot the distance of peak-delay $\Delta L/d$ depending on the Reynolds number in Fig. 13. At small Reynolds numbers, the peak-delay is about $(0 \div 2)d$. We observed the nonlinearity of the peak-delay behavior as well.

4. Conclusions. In this paper, we present Lorentz force measurements of a spherical particle rising in liquid metal initially at rest. The analytical solu-

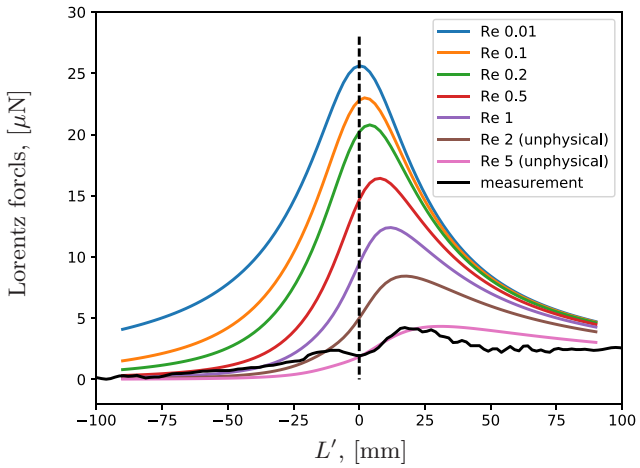

Fig. 12. Lorentz force signals in simulation and experiment.

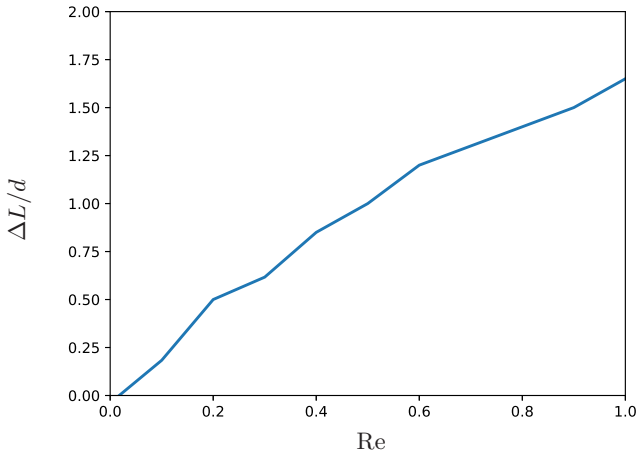

Fig. 13. The normalized delay of the peaks of Lorentz force signals.

tion of the flow around a moving sphere is applied in our numerical model, and the Lorentz forces are compared to experiments. In view of many simplifications, the peak values of the Lorentz force from the analytical velocity fields provide the upper-limit for the measurement results. The peak-delay of the Lorentz force is observed by both experiments and simulations, where we see its nonlinear dependence on the Reynolds number. Although the numerical model is physical only in the cases of low Reynolds numbers, it provides reasonable estimation of the Lorentz force behavior in the experiments. Accurate CFD simulations will be required to reproduce the force signals quantitatively.

Acknowledgements. We acknowledge financial support from the Deutsche Forschungsgemeinschaft (DFG) in the framework of the Research Training Group GRK 1567 “Lorentz Force Velocimetry and Lorentz Force Eddy Current Testing” and Helmholtz Alliance LIMTECH within the seed grant program of Young Investigators Group. We are also thankful to T. Wondrak for fruitful discussions on the experimental design and to N. Tran and D. Hernández for their help on the simulation.

References

[1] J.A. Shercliff. *The theory of Electromagnetic Flow-Measurement* (Cambridge University Press, 1987).

[2] A. Thess, E. Votyakov, and Y. Kolesnikov. Lorentz force velocimetry. *Physical Review Letters*, vol. 96 (2006), no. 16, p. 164501.

[3] C. Heinicke and T. Wondrak. Spatial and temporal resolution of a local lorentz force flowmeter. *Measurement Science and Technology*, vol. 25 (2014), no. 5, p. 055302.

[4] P.A. Davidson. *An Introduction to Magnetohydrodynamics* (Cambridge University Press, 2001). .

[5] Z. Lyu and C. Karcher. Non-contact electromagnetic flow measurement in liquid metal two-phase flow using Lorentz force velocimetry. *Magnetohydrodynamics*, vol. 53 (2017), no. 1, pp. 67–77.

[6] R. Füssl and G. Jäger. The influence of the force feed-in system on high-accuracy low force measurement. In *XIX IMEKO World Congress Fundamental and Applied Metrology, Lisbon, Portugal* (2009).

[7] A. Thess, E. Votyakov, B. Knaepen, and O. Zikanov. Theory of the Lorentz force flowmeter. *New Journal of Physics*, vol. 9 (2007), no. 8, p. 299.

[8] E.P. Furlani. *Permanent Magnet and Electromechanical Devices: Materials, Analysis, and Applications* (Academic Press, London, UK., 2001).

[9] H. Lamb. *Hydrodynamics.* (Cambridge University Press, 1932).

[10] I.J. Veysey and N. Goldenfeld. Simple viscous flows:from boundary layers to the renormalization group. *Reviews of Modern Physics*, vol. 79 (2007), no. 3, p. 883.

[11] S. Taneda. Experimental investigation of the wake behind a sphere at low Reynolds numbers. *Journal of the Physical Society of Japan*, vol. 11 (1956), no. 10, pp. 1104–1108.

Received 08.12.2017